Published in final edited form as:

J Neurochem. 2016 October ; 139(1): 40–54. doi:10.1111/jnc.13738.

Novel molecular insights into the critical role of sulfatide in myelin maintenance/function

Juan Pablo Palavicini[1,#], **Chunyan Wang**[1,#], **Linyuan Chen**[1], **Sareen Ahmar**[1], **Juan Diego Higuera**[1], **Jeffrey L. Dupree**[2,3], and **Xianlin Han**[1,*]

[1]Center for Metabolic Origins of Disease, Sanford Burnham Prebys Medical Discovery Institute, Orlando, Florida 32827

[2]Department of Anatomy and Neurobiology, Virginia Commonwealth University, Richmond, Virginia 23298

[3]Research Division, McGuire Veterans Affairs Medical Center, Richmond, VA 23249

Abstract

Cerebroside sulfotransferase (CST) catalyzes the production of sulfatide, a major class of myelin-specific lipids. CST knockout ($CST^{-/-}$) mice in which sulfatide is completely depleted are born healthy, but display myelin abnormalities and progressive tremors starting at 4–6 weeks of age. Although these phenotypes suggest that sulfatide plays a critical role in myelin maintenance/function, the underlying mechanisms remain largely unknown. We analyzed the major CNS myelin proteins and the major lipids enriched in the myelin in a spatiotemporal manner. We found a one-third reduction of the major compact-myelin proteins (myelin basic protein, MBP, and proteolipid protein, PLP) and an equivalent post-developmental loss of myelin lipids, providing the molecular basis behind the thinner myelin sheaths. Our lipidomics data demonstrated that the observed global reduction of myelin lipid content was not due to an increase of lipid degradation but rather to the reduction of their synthesis by oligodendrocytes. We also showed that sulfatide depletion leads to region-specific effects on non-compact myelin, dramatically affecting the paranode (neurofascin 155) and the major inner-tongue myelin protein (myelin-associated glycoprotein). Moreover, we demonstrated that sulfatide promotes the interaction between adjacent PLP extracellular domains, evidenced by a progressive decline of high molecular weight PLP complexes in $CST^{-/-}$ mice, providing an explanation at a molecular level regarding the uncompacted myelin sheaths. Finally, we proposed that the dramatic losses of neurofascin 155 and PLP interactions are responsible for the progressive tremors and eventual ataxia. In summary, we unraveled novel molecular insights into the critical role of sulfatide in myelin maintenance/function.

[*]To whom correspondence should be addressed: Xianlin Han, Ph.D., Center for Metabolic Origins of Disease, Sanford Burnham Prebys Medical Discovery Institute, 6400 Sanger Road, Orlando, Florida 32827, Telephone: (407) 745-2139, Fax: (407) 745-2016, xhan@sanfordburnham.org.

[#]Authors contributed equally

Conflict of interest disclosure

The authors have no conflict of interest to declare.

Keywords

cerebroside sulfotransferase; myelin-associated glycoprotein; myelin lipidome; proteolipid protein; shotgun lipidomics; sulfatide

Introduction

The myelin sheath is a multilamellar, spirally wrapping extension of the plasma membrane of oligodendrocytes (OLs) in the central nervous system (CNS). Myelin composition is characterized by remarkably high lipid levels which account for 70–75% of its dry weight, complemented with a relatively simple array of myelin-specific proteins. Myelin has a characteristic lipid composition that distinguishes it from other cellular membranes. Even though there are no absolute "myelin-specific" lipids, galactosylceramide (GalCer) and its sulfated form, sulfatide (ST), are the most typical lipids of myelin. In fact, the concentration of GalCer in the brain is directly proportional to the amount of myelin present (Norton & Poduslo 1973). In addition to galactolipids, the major lipids of myelin are cholesterol and ethanolamine-containing plasmalogens (Quarles 2007; Siegel *et al.* 1999; Han *et al.* 2001). Phosphatidylethanolamine and phosphatidylcholine are also major myelin constituents, whereas sphingomyelin represents a relatively minor component. Not only is the general lipid composition of myelin highly characteristic, the fatty acid composition of many of the individual lipid classes is also distinctive (Siegel et al. 1999; Han et al. 2001).

Moreover, myelin has an exclusive protein composition, being highly enriched in proteolipid protein (PLP) and myelin basic protein (MBP), which together account for >50% of protein content and constitute the major components of compact CNS myelin (Campagnoni & Skoff 2001). Both PLP and MBP have positively charged intracellular surfaces that mediate their interaction with the negatively charged myelin membrane, explaining their function as membrane adhesion and myelin compaction proteins (Campagnoni & Skoff 2001). MBP is an intracellular membrane protein, while PLP is a hydrophobic integral membrane protein which is also involved in the myelin intraperiod line formation connecting adjacent myelin layers, presumably through extracellular PLP-PLP interactions (Greer & Lees 2002). The major non-compact myelin proteins include cyclic nucleotide phosphodiesterase (CNP) (Rasband *et al.* 2005) and NAD-dependent deacetylase sirtuin-2 (SirT2) (Southwood *et al.* 2007). The paranodal myelin loop is enriched with neurofascin 155 (NF155) (Kriebel *et al.* 2012), while the most abundant inner and outer myelin tongue proteins are myelin-associated glycoprotein (MAG) (Quarles 2007) and myelin-oligodendrocyte glycoprotein (MOG) (Roth *et al.* 1995), respectively.

ST, a class of sulfated GalCer, is predominantly synthesized by OLs in the CNS and is highly enriched in the myelin sheath (Takahashi & Suzuki 2012), where it makes up about a third of total galactolipids (Wang *et al.* 2014). ST possesses sphingoid backbone moieties and different lengths of acyl chains which can be hydroxylated (Takahashi & Suzuki 2012). A ST-deficient mouse model has been generated by disrupting the gene that encodes the enzyme cerebroside sulfotransferase (CST) that catalyzes the last step of ST biosynthesis (Honke *et al.* 2002). CST knockout ($CST^{-/-}$) mice, which show a complete loss of ST in

brain tissue, are born healthy, but begin displaying hindlimb weakness and tremors by 4–6 weeks of age. These defects aggravate with age, causing pronounced tremor and eventual ataxia, that lead to partial or complete paralysis by 12 months of age and eventually result in premature death which typically occurs around 15 months (Honke *et al.* 2002). Ultrastructural axonal analysis has revealed that although myelin develops quite normally, these mice show thinner and less compacted myelin sheaths, deteriorated nodal structure, reduced axon caliber and circularity, and reduced conduction velocities with age (Honke et al. 2002; Marcus *et al.* 2006; Hayashi *et al.* 2013). However, the molecular mechanisms by which ST depletion leads to these myelin phenotypes remain largely unknown. Considering that in mice myelination starts during the first postnatal week and peaks at ~21 days after birth (Benjamins & Morell 1978; Foran & Peterson 1992), the above described studies from $CST^{-/-}$ mice strongly indicate that (1) either ST is not critical for myelin development or its deficiency is somehow compensated, and (2) ST plays a major role in myelin maintenance (Marcus *et al.* 2006).

Altered mass levels of ST in the human brain are involved in the pathogenesis of various human diseases. Accumulation of ST due to deficiency in arylsulfatase A, a lysosomal enzyme that catalyzes ST degradation, causes metachromatic leukodystrophy (MLD). MLD is an autosomal recessively inherited lysosomal storage disorder characterized pathologically by progressive demyelination that leads to ataxia and other neurological symptoms (Eckhardt *et al.* 2007). In addition, a dramatic and specific deficiency in ST content is present in Alzheimer's disease (AD) at the earliest clinically recognizable stages (Han *et al.* 2002; Svennerholm & Gottfries 1994). Severe sulfatide deficiency has also been reported for multiple AD animal models (Cheng *et al.* 2010). We have revealed that this reduction is mediated by apolipoprotein E, the major genetic factor linked to AD, which was associated with ST trafficking, metabolism, and homeostasis in an isoform-dependent manner (Han 2007; Han *et al.* 2003).

In the current study, we aimed to unravel novel molecular insights into the role of ST in myelin maintenance. For that purpose, we investigated the spatiotemporal effects of CST gene disruption on CNS myelin lipid and protein homeostasis by multi-dimensional mass spectrometry-based shotgun lipidomics (MDMS-SL) (Han *et al.* 2012; Wang *et al.* 2016a; Yang *et al.* 2009) and biochemical approaches, respectively, using brain and spinal cord tissue. We unraveled novel molecular fingerprints underlying the myelin phenotypes described for CST KO mice, including (1) a one-third loss of compact-myelin proteins and major myelin lipids, presumably due to the loss of negative charges from ST species, (2) a striking post-developmental loss of MAG and NF155, and (3) a progressive loss of intermolecular PLP interactions. Finally, we proposed that the tremor and ataxic phenotypes that occur in the absence of ST are a consequence of the loss of NF155 and PLP intermolecular interactions.

Methods

Mice

CST mice ($CST^{+/+}$, $CST^{+/-}$, and $CST^{-/-}$) on a C57BL/6J background were housed in groups of ≤5 mice/cage, maintained in a temperature- and humidity-controlled environment with a

12-h light-dark cycle, and provided with food and water *ad libitum*. Male CST mice (1- to 10-months old) were euthanized by asphyxiation with CO_2 followed by decapitation. Brain regions and spinal cords were immediately dissected and frozen before analysis. The protocols for animal experiments were conducted in accordance with the "Guide for the Care and Use of Laboratory Animals" (8th edition, National Research Council of the National Academies, 2011) and were approved by the Animal Studies Committee of Sanford Burnham Prebys Medical Discovery Institute.

Lipid extraction

Brain and spinal cord frozen tissues (15 mg each) were weighed and homogenized in 1 ml of ice-cold diluted phosphate-buffered saline (0.1× PBS) with a Potter-Elvehjem tissue grinder. Protein assays on individual homogenates were performed using a BCA protein assay kit (Pierce, Rockford, IL, USA). Lipids were extracted by a modified procedure of Bligh and Dyer extraction as described previously (Cheng *et al.* 2006; Cheng *et al.* 2007) in the presence of internal standards which were added based on total protein content of the sample (for details see Supporting Information).

Mass spectrometric analysis of lipids

A triple-quadrupole mass spectrometer (Thermo Scientific TSQ Vantage, CA, USA) equipped with a Nanomate device (Advion Bioscience Ltd., NY, USA) and Xcalibur system software was used as previously described (Han *et al.* 2008; Yang et al. 2009). Diluted lipid extracts were directly infused into the ESI source through a Nanomate device (Han *et al.* 2008). Typically, signals were averaged over a 1-min period in the profile mode for each full scan MS spectrum. For tandem mass spectrometry, a collision gas pressure was set at 1.0 mTorr, but the collision energy varied with the classes of lipids as described previously (Yang et al. 2009; Han & Gross 2005). Similarly, a 2- to 5-min period of signal averaging in the profile mode was employed for each tandem mass spectrum. All full and tandem mass spectra were automatically acquired using a customized sequence subroutine operated under Xcalibur software.

Data processing including ion peak selection, baseline correction, data transfer, peak intensity comparison, ^{13}C deisotoping, and quantitation were conducted using a custom programmed Microsoft Excel macro as previously described (Yang *et al.* 2009) after considering the principles of lipidomics (Wang *et al.* 2016b; Han 2016).

Western blotting

Brain or spinal cord frozen tissue (20 mg each) was homogenized in 1× NP40 with a hand-held homogenizer and briefly sonicated with a Branson Sonifier®. NP40 homogenates were centrifuged at 12,300 rpm for 20 min at 4 °C and supernatants were run into NuPage 4–12% Bis-Tris or NuPage Tris-Acetate gels (Life Technologies, NY, USA) under reducing conditions. Samples were normalized based on total protein content, which was estimated by BCA protein assay. Western blot analyses were performed using antibodies against PLP1 (Rabbit, Sigma, MO, USA), MBP (Rabbit, GenScript, NJ, USA), MOG (Rat, R&D Systems, MN, USA), MAG (Rabbit, Cell Signaling, MA, USA), CNPase (Rabbit, Cell Signaling,

MA, USA). Relative intensities were quantified using ImageJ software and normalized to a loading control (GAPDH).

Immunofluorescence

Mouse brains were dissected, fixed in 4% PFA, cryoprotected, embedded in OCT, and frozen. Cryostat brain sections (8 μm) were mounted on positively charged slides. Tissue-containing slides were incubated with anti-MAG (rabbit monoclonal antibody, Cell Signaling) or anti-CNP (rabbit monoclonal antibody, Cell Signaling) primary antibodies overnight at 4 °C and incubated with secondary antibody (Goat anti-rabbit Alexa Fluor® 647) for 1 h at room temperature, following by addition of DAPI-containing mounting media (Vectashield, Vector Laboratories). Images were taken using a Nikon A1R VAAS inverted confocal microscope and analyzed using NIS-Elements imaging software (Nikon). Data analysis involved quantification of 3 equally spaced brain coronal sections from 4 different animals per genotype.

Statistical analysis

Quantitative data were normalized to protein content and were presented as the means ± SE. Differences between mean values were determined by unpaired Student's *t* test (one time point analysis comparing the abundance of specific lipid species or protein between the 3 different genotypes), and 2-way ANOVA (multiple time points comparing the total class content between the 3 different genotypes) using GraphPad Prism software. Lipidomic profiling data were log-10 transformed for partial least squared-discriminatory analysis (PLS-DA) with SIMCA-P software and for hierarchical clustering analysis using Euclidean dissimilarity and average linkage with Partek Genomics Suite software.

Results

Sulfatide depletion leads to a disruption of myelin lipid homeostasis following myelin development

To investigate the effects of ST in CNS myelin lipid homeostasis post-developmentally, we determined the spinal cord lipidomes of adult (i.e., 3 months old) CST+/+, +/− and −/− mice by MDMS-SL, given that the myelin and tremor phenotypes are already evident at 3 months of age and that spinal cord is the most white matter-rich CNS region. As expected, $CST^{-/-}$ mice were completely deprived of ST, while $CST^{+/-}$ mice had ~80% the amount of total ST from $CST^{+/+}$ mice (Fig. 1a and c). Considering that ST is a class of sphingolipid, we hypothesized that the levels of other myelin-enriched sphingolipids could be affected in ST deficient mice. Surprisingly, we found that ST precursor, GalCer, which is abundantly present in the CNS, was significantly decreased (a reduction of ~20%) in ST-depleted spinal cords (Fig. 1b and d). These results suggest that the loss of ST results in reduced GalCer synthesis and/or increased GalCer degradation, since otherwise GalCer would actually be expected to accumulate given that GalCer is the precursor of ST biosynthesis. Next, we analyzed a second myelin-enriched sphingolipid class, i.e., sphingomyelin (SM), which shares the same ceramide backbone as GalCer, and found that total SM levels were also significantly decreased (a reduction of ~25%) in the absence of ST (Fig. 1e). These results

strongly support the notion that ST plays a major role as a regulator of sphingolipid synthesis that is critical for myelin maintenance.

Detailed analysis of individual sphingolipid species revealed a very similar distribution of individual species for ST, GalCer, and SM. For each analyzed sphingolipid class, the most abundant lipid species was composed of a ceramide possessing 4-sphingenine (*d*18:1) and nervonic acid (24:1 fatty acid), accounting for ≥30% of the total class content (Fig. 1a–b). Notably, CST deficiency had specific effects on individual sphingolipid species, and those effects were shared among sphingolipid classes. For example, the most abundant sphingolipid species (*d*18:1/24:1) was reduced by ~25% in the absence of ST in both GalCer and SM, while mild/low abundance sphingolipid species were either similarly reduced (*d*18:1/20:0, *d*18:1/22:0, ~30% reduction), reduced even further (*d*18:1/22:1, ~50% decrease), or not significantly altered (*d*18:1/18:0 and *d*18:1/24:0). The fact that ST depletion had virtually identical effects on different sphingolipid classes is completely consistent and supportive of a reduction in global sphingolipid synthesis. In summary, we demonstrated that ST depletion leads to a post-developmental disruption of myelin sphingolipid homeostasis.

Given the strong post-developmental effect of ST depletion on myelin sphingolipid homeostasis, we proceeded to determine its effects on myelin phospholipid homeostasis in adult spinal cords by MDMS-SL. Surprisingly, ST depletion also led to a significant decrease in every major myelin phospholipid class (Fig. 2). Specifically, total ethanolamine plasmalogen was significantly reduced (12%) (Fig. 2a); while the total content of the remaining major myelin phospholipid classes: phosphatidylserine (PS), phosphatidylethanolamine (PE) (excluding ethanolamine plasmalogen), and phosphatidylcholine (PC); were reduced even more extensively (45%, 35%, and 30%, respectively) (Fig. 2b–d). Detailed analysis of specific lipid species from each phospholipid class revealed that the vast majority of the species were either extensively or mildly reduced, while only a few species were not altered. Notably phospholipids containing 18:0 and 18:1 fatty acids (FAs) were particularly sensitive to the absence of ST since most of them were extensively decreased in the absence of ST (Figs. S1–S3). This is consistent with the fact that 18:0 and 18:1 FAs are particularly abundant in white matter (OL myelin membranes) (Han *et al.* 2001). On the other hand, phospholipid species containing polyunsaturated fatty acyl constituents were generally not altered in the absence of ST, consistent with the fact that they are particularly abundant in gray matter (neuronal membranes) (Han *et al.* 2001) (Figs. S1–S3).

Decreased levels of myelin phospholipids must be explained by decreased OL phospholipid synthesis and/or increased degradation. Increased phospholipid degradation is typically accompanied by an accumulation of phospholipase cleavage products, e.g., lysophospholipids (LPLs). Thus, we proceeded to quantify the levels of the two major LPL classes, i.e., lysophosphatidylethanolamine and lysophosphatidylcholine, under ST depleted conditions. No significant differences were found in the levels of total LPLs under ST depleted conditions (data not shown). Taken together, our data strongly implicate ST as a key mediator of OL phospholipid synthesis critical for myelin maintenance.

Finally, we tested the levels of free cholesterol in adult CST spinal cords. Consistent with our sphingolipid and phospholipid results, a significant decrease in the levels of cholesterol in $CST^{-/-}$ compared to $CST^{+/+}$ or $CST^{+/-}$ mice (~20%) was also determined. In summary, with no exception ST depletion led to a significant decrease in all the major lipid classes enriched in myelin.

It is important to mention that those myelin lipid classes whose content was extensively reduced (≥35%) in $CST^{-/-}$ were also mildly reduced in $CST^{+/-}$ mice, while those lipid classes whose content was only mildly reduced (≤35%) in $CST^{-/-}$, were not altered in $CST^{+/-}$ mice. For example, total PS content decreased quite dramatically in $CST^{-/-}$, while it was mildly reduced in $CST^{+/-}$ mice (Fig. 2b). On the other hand, total GalCer was only mildly reduced in $CST^{-/-}$, while it was not significantly decreased in $CST^{+/-}$ mice (Fig. 1d). This trend was also true for specific lipid species. Those species that were extensively altered in the complete absence of ST tended to be mildly reduced in ST deficient conditions. These results support a strong dose dependent effect between ST content and overall myelin lipid content, where decreased ST levels lead to an overall decrease in total myelin lipids in a post-developmental manner. Taken together, our spinal cord lipidomics data from adult CST mice clearly demonstrated that ST deficiency significantly affects OL synthesis of myelin lipids.

Spatiotemporal effects of sulfatide depletion on myelin lipid homeostasis

To better understand the effects of ST deficiency on myelin lipid homeostasis, we expanded our initial spinal cord lipidomics analysis to incorporate brain tissue (i.e., cerebellum and cortex). While the spinal cord tissue is highly enriched in white matter, the cerebellum has similar amounts of white and gray matter, and the cortex is highly enriched in gray matter. In addition, considering that during myelin development (i.e., first 3–4 postnatal weeks) no significant effects were observed in the lipidomes of these CNS regions under ST depleted conditions (Wang *et al.* 2014), we were interested in investigating the temporal effects of ST deficiency on myelin lipid homeostasis.

We found that total ST content in $CST^{+/-}$ mice was 60–80% of that of $CST^{+/+}$ throughout all time points (1–10 months) in the three CNS regions examined. Interestingly, at 3 months of age we saw the lowest levels of ST content in $CST^{+/-}$ mice in all CNS regions (Fig. 3a). In addition, GalCer content was reduced by 20–40% in all the CNS regions of 3 months or older $CST^{-/-}$ compared to $CST^{+/+}$ mice. Again, the most dramatic effects were observed at 3 months in brain tissue (up to 40% decrease), where even $CST^{+/-}$ showed a slight but significant decrease in total GalCer content (up to 15% decrease) (Fig. 3b). Notably, the effects of ST depletion on GalCer content did not progress with age since very similar consequences were observed in 5 and 10 months old $CST^{-/-}$ mice compared to $CST^{+/+}$ or $CST^{+/-}$ littermates. Interestingly, although total SM levels were decreased after 3 months of age in spinal cord, they were not altered in any of the two brain regions tested at any myelin maintenance stage (Fig. 3c). These results are consistent with the fact that GalCer is highly specific to myelin, while SM is a significant component of both myelin and neuronal cell membranes.

The spatiotemporal effects of ST deficiency on phospholipid homeostasis paralleled to those observed for sphingolipids. Total PE and PS contents were significantly reduced in all CNS regions analyzed for 3-months and older $CST^{-/-}$ mice (Fig. 3d and f). Again, the effects of ST depletion on phospholipid homeostasis did not progress with age, yielding very similar consequences at 5 and 10 months of age (Fig. 3d and f). Although total PC was also significantly decreased in $CST^{-/-}$ spinal cords, total levels were not altered in any of the two brain tissues or time points analyzed (Fig. 3e). These results are consistent with the fact that PE plasmalogens and PS are both highly enriched in white matter, while PC is abundant in both white and gray matter. Finally, a very similar trend to that described for phospholipids was observed for total cholesterol, where no changes were detected at one month of age, and similar reductions were seen between 3- and 10-months of age (15–25%). In summary, our data evidenced that ST depletion specifically alters myelin lipid homeostasis in a post-developmental manner and that this effect does not aggravate as mice age.

The effects of sulfatide depletion on lipid homeostasis are specific to myelin lipids

The results from our analysis on multiple CNS regions strongly support the idea that ST effects on lipid homeostasis are specific to OL-produced lipids. To further validate this notion, multivariate profile-wide predictive models were constructed using partial least square-discriminate analysis (PLS-DA) for individual lipid classes to generate score scatter loading plots using our lipidomics data from adult mice cerebella (Fig. S4). As expected, analysis of specific lipid classes revealed that $CST^{-/-}$ mice clustered together, while $CST^{+/+}$ and $CST^{+/-}$ mice formed a second separate cluster (Fig. S4). Notably, even though the total levels of SM and PC were not altered in the brains of adult $CST^{-/-}$ mice (Fig. 3c and e), PLS-DA revealed that $CST^{-/-}$ mice still clustered together away from $CST^{+/+}$ and $CST^{+/-}$ mice (Fig. S4a and c). Thus, a subset of specific lipid species must be responsible for the effects observed in the PLS-DA scatter plots of SM and PC. On the other hand, the more dramatic effects seen on PE and PS PLS-DA scatter plots (note the higher % values for t[1]) are due to a more global effect that involves a bigger set of lipid species within each class (Fig. S4b and d). In summary, our PLS-DA results further evidenced that the effect of ST depletion on lipid homeostasis was specific to a subset of brain lipids, those present in the myelin.

To further validate this assertion, we took advantage of the differential myelin content between the three examined CNS regions (i.e., spinal cord, cerebellum, and cortex). As expected, wildtype spinal cord contained ~5-fold more myelin than cerebellum, while cerebellum contained ~3-fold more myelin than brain cortex. Such calculations were made based on the total levels of GalCer and ST on each CNS region in wildtype mice, since these galactolipids are almost exclusively present in myelin. This approach allowed us to identify molecular lipid species that are more abundant in white matter compared to gray matter. Consistent with our hypothesis, we noticed that the vast majority of molecular species that were decreased in the absence of ST had high [cerebellum]/[cortex] ratios (CBL/CX), while the vast majority of molecular species that were not significantly altered in the absence of ST had low CBL/CX ratios (Figs. S1–S3). Furthermore, we set up a threshold CBL/CX ratio to classify individual molecular species as “myelin enriched” (CBL/CX ratio >2) or “non-myelin enriched” (CBL/CX ratio <2). Notably, the total content of the “myelin-enriched”

species of the major myelin phospholipid classes (PE, PC, and PS) was significantly reduced for all phospholipid classes in ST depleted mice, while the total content of "non-myelin-enriched" species was either not or only slightly altered (Fig. S5a–c).

Previous work comparing the fatty acid (FA) composition between mouse myelin and neuronal membranes has revealed that the most abundant FA chains for phospholipids in myelin are 18:1 and 18:0, which together make up more than 50% of total FA content in the myelin (Chrast *et al.* 2011). The most abundant phospholipid FA in myelin, 18:1, in addition 20:0, 22:0, 24:0, and 24:1 have also been shown to be strongly enriched in myelin compared to other membranes; while 18:2, 20:4 and 22:6 are particularly infrequent in the myelin (Chrast et al. 2011; Han et al. 2001). Careful examination of individual lipid species for each phospholipid class in brain tissue revealed that virtually all significantly altered lipid species under ST deficient conditions contained both or at least one of the above mentioned myelin-enriched FAs (Figs. S1–S3). In contrast, none of the brain lipid species that contained two FAs known to be in low abundance in myelin was altered (Figs. S1–S3). In summary, detailed analysis of specific lipid species within major lipid classes confirmed that ST depletion leads to a specific decrease of lipids within the myelin membrane without affecting lipids within neuronal membranes.

Sulfatide depletion leads to a selective and dramatic reduction of major myelin proteins

The fact that ST depletion led to a clear decrease of myelin-specific lipids post-developmentally together with our previous observation that $CST^{-/-}$ mice show a significant reduction in myelin thickness compared to littermate controls (Marcus *et al.* 2006) prompted us to speculate that ST depletion could also disrupt myelin protein homeostasis in adult mice.

The first evidence supporting this idea came from the observation that total protein content per mg of spinal cord in $CST^{-/-}$ mice was significantly lower (~25%) compared to that of $CST^{+/+}$ or $CST^{+/-}$ (Fig. 4a). On the other hand, total protein content per mg of cerebellum or cortex was not altered in ST-depleted animals, consistent with their much lower white to gray matter ratios (Fig. 4a). Although no significant differences were found in the levels of the two major myelin proteins in ST-depleted spinal cords, significant differences were found in brain tissues (Fig. 4b–c). The two most abundant myelin-specific proteins, PLP and MBP, were significantly reduced by ~25% in 3 months old $CST^{-/-}$ cerebellar (Fig. 4b–c) and cortical tissue (not shown). Notably, a similar degree of reduction was observed in spinal cord samples when normalized against tissue weight instead of total protein content (not shown). In other words, the reduction in total protein content observed in $CST^{-/-}$ spinal cords seems to be mostly due to the loss of PLP and MBP proteins which together make up more than 50% of myelin protein content (Campagnoni & Skoff 2001).

Since ST depletion led to a reduction of the two major myelin-specific proteins, we wondered whether other major myelin proteins were also affected by ST absence. ST depletion did not have any effect on the levels of CNP in brain or spinal cord homogenates, the third major myelin-specific protein, when assessed by Western blotting (Fig. 4b–c). Next, we proceeded to analyze the effects of ST deficiency on MOG and MAG, two major non-compact myelin-specific proteins that are restricted to the outer and inner internodal

layers, respectively. Strikingly, we found that ST deficiency led to a dramatic reduction of MAG content (~80%) in adult mouse brains while MOG levels were not altered (Fig. 4b–c). MAG levels were also significantly reduced in adult spinal cord samples after being normalized for either total protein content or weight tissue (~55% and ~80%, respectively). Notably, we validated our biochemical results by immunohistochemistry, where an evident reduction of MAG levels was also observed in every CNS region examined, including forebrain, cerebella (Fig. 5a–b), and spinal cord. In addition, consistent with our previous report (Pomicter *et al.* 2013), we found a striking reduction in the levels of the paranodal-specific NF155 protein in $CST^{-/-}$ mice (Fig. 4b–c).

Although the widespread decrease in myelin lipids seen in $CST^{-/-}$ mice could potentially be explained by a decrease in OL production, the specific effects of ST depletion on myelin proteins did not support such possibility. To further clarify this, we measured the levels of NG2 chondroitin sulfate, a marker of OL precursor cells; and Olig2, a transcription factor expressed in both immature and mature OLs within brain and spinal cord homogenates of adult mice. CST depletion did not result in any alteration of these OL markers (Fig. 4b–c). In fact, $CST^{-/-}$ mice showed higher numbers of Olig2+ cells within the spinal cord during early development (Shroff *et al.* 2009). Interestingly, myelin regions from $CST^{-/-}$ mice showed more intense CNP staining than WT littermates (Fig. 6a, c, and d); however this staining was constrained within a smaller white matter region (Fig. 6b and e). This pattern is consistent with the increased number of mature OLs but reduced white matter tract area reported for $CST^{-/-}$ mice in previous studies (Shroff et al. 2009; Hirahara *et al.* 2004), as well as for $CGT^{-/-}$ mice, which lack both ST and GalCer (Bansal *et al.* 1999; Marcus *et al.* 2000).

Finally, we analyzed the effects of ST depletion on specific myelin proteins in a longitudinal manner. Compact myelin-proteins (PLP and MBP) in ST-depleted animals were reduced early on in the cerebellum and slightly later in the spinal cord, however such reductions were not progressive (Fig. S6a–b). On the other hand, MAG content was slightly reduced at 1 month of age in all the CNS regions examined, and although its levels dramatically decreased between 1–3 months of age, they did not decreased further as mice aged (Fig. S6c). Finally, the non-compact myelin proteins CNP, SirT2, and MOG, as well as the pre- and mature OL marker Olig2, were not altered at any CNS region or time point analyzed (not shown). In summary, we demonstrated that ST depletion leads to an early dysregulation of compact myelin proteins and a disruption of periaxonal inner tongue structure, none of which aggravate as adult mice age.

Sulfatide mediates intraperiod line and myelin-axon junction interactions

Glial NF155 mediates the myelin-axon junction via its association with the axonal Caspr-contactin complex. ST depletion led to a dramatic and progressive loss of NF155 in every CNS region analyzed (Fig. S6d). Importantly, the age-dependent effect on PLP dimerization and NF155 levels paralleled to the age-dependent loss of myelin compactness in ST-depleted animals, as well as the development of tremor and ataxic phenotypes characteristic of $CST^{-/-}$ mice that start at ~4 weeks, become evident at 6 weeks and lead to partial paralysis at ≥10 months of age as previously reported (Honke *et al.* 2002).

PLP interacts extracellularly with other PLP chains from the surface of the myelin membrane in the next loop of the spiral. Such PLP interactions are evidenced by the presence of high molecular weight (HMW) band(s) present in Western blots, which vary in number and size depending on the specific PLP antibody used and running conditions, and represent a combination of full length and/or cleaved PLP homo- and hetero-dimers and oligomers (Daffu *et al.* 2012; Swanton *et al.* 2005). Under our experimental conditions, high exposure of PLP Western blots revealed a defined HMW band migrating at ~37 kDa (putative dimer) as well as a set of higher molecular weight bands that migrated as a smear (putative oligomers), in addition to the PLP/DM20 monomer bands that migrated at ~25/20 kDa (Fig. S6e–f). Putative PLP dimer and oligomer bands were progressively reduced in the absence of ST in an age dependent manner (Fig. S6e–f). Quantification of the putative PLP dimer band (~37 kDa) revealed a ~40% reduction in 1 month old $CST^{-/-}$ mouse brains, which became more extensive as the animals aged, reaching a dramatic 80% decrease by 5 months of age, and an almost complete absence in ≥10 months old mice (Fig. S6f).

Discussion

ST plays a critical role in maintaining myelin lipid homeostasis

We have previously demonstrated that during myelin development (i.e., first 3–4 postnatal weeks), CST-depleted mice show no structural myelin alterations (Marcus *et al.* 2006) and no evident lipid homeostasis alterations (Wang *et al.* 2014). However, following myelin development (≥1 months of age) multiple myelin phenotypic abnormalities become evident in adult $CST^{-/-}$ mice, including thinner and less compacted myelin sheaths as well as nodal and paranodal deterioration (Marcus *et al.* 2006). Therefore, we hypothesized that ST depletion could lead to altered myelin-lipid homeostasis in a post-developmental manner. Consistent with our previous ultrastructural findings, herein we reported for the first time that ST plays a role in myelin lipid homeostasis. Importantly, ST deficiency had a widespread post-developmental effect on the levels of all major myelin lipids, reducing the levels of sphingolipids (GalCer and SM), phospholipids (PE, PC, and PS), and cholesterol (Figs. 1–3). Given that ST is a myelin-enriched lipid and that all of the specific lipid classes altered in the absence of ST are also enriched in myelin, it seems reasonable to predict that the role of ST on maintaining lipid homeostasis would be specific to myelin lipid synthesis by OLs. Evidence supporting this notion came from comparisons between different CNS regions containing low, mid, and high contents of myelin (i.e., cortex, cerebellum, and spinal cord) and from detailed analysis of individual molecular species from each major lipid class, which evidenced that ST exclusively modulates myelin-enriched lipid species (Figs. 1–3 and Figs. S1–S5). In summary, myelin lipids were significantly reduced in the absence of ST in a post-developmental manner, while non-myelin lipids were not altered. Overall, CNS myelin lipids were all reduced to a similar extent (by about one third) in the absence of ST following myelin development, an effect that did not aggravate with age.

Moreover, we provided strong evidence supporting the notion that ST depletion reduces myelin lipid content by downregulating myelin lipid synthesis and demonstrated that such effect is not due to the degradation of myelin lipids. Specifically, we confirmed that phospholipid cleavage products do not accumulate in ST depleted conditions. We proposed

that the widespread effects on sphingolipids, phospholipids, and cholesterol under ST depleted conditions likely result from an upstream inhibition of the global lipid synthesis machinery. Thus, our data strongly support a novel role for ST as a master regulator of OL lipid biosynthesis during myelin maintenance. Importantly, our findings are consistent with the previously proposed role of ST as a regulator of late OL differentiation (Bansal *et al.* 1999). Consistent with this hypothesis, perturbation with specific anti-sulfated glycolipid antibodies or liposomes containing ST, as well as inhibition of ST synthesis in culture, resulted in alterations of OL differentiation and the maintenance of myelin-like membranes (Bansal *et al.* 1988; Bansal et al. 1999; Dyer & Benjamins 1988; Bansal & Pfeiffer 1989; Boggs & Wang 2001). To the best of our knowledge, this is the first report demonstrating that ST regulates global myelin lipid homeostasis *in vivo*.

ST plays a critical role in maintaining compact myelin, nodal and paranodal homeostasis

Although ST deficiency has not been shown to alter major myelin-specific proteins during myelin development (Fewou *et al.* 2010; Pomicter *et al.* 2010), considering the global post-developmental effects described for myelin lipids, we wondered whether ST depletion also affects myelin-specific proteins in adult mice. We found that ST depletion led to significant alterations in several major myelin-specific proteins. Specifically, compact-myelin proteins (PLP and MBP) were significantly reduced in $CST^{-/-}$ brain tissue (Figs. 4 and S6). Notably, compact-myelin proteins were reduced to a similar extent to that observed for myelin lipids (by about one third), a reduction that was also not aggravated with age. Interestingly, mild reductions of compact myelin proteins were already evident by 1–3 months in different CNS regions. Importantly, the described losses of both myelin lipids and compact-myelin proteins parallel the loss of myelin thickness previously reported for $CST^{-/-}$ mice (Marcus *et al.* 2006).

Furthermore, consistent with a previous study where we demonstrated that two major non-compact myelin proteins, i.e., NF155 and MAG, are specifically susceptible to detergent extraction in the absence of ST (Pomicter *et al.* 2013), here we reported that the total levels of MAG were dramatically reduced in the absence of ST following myelin development, an effect that did not aggravate with age (Figs. 4, 5, and S6). NF155 levels were dramatically and progressively reduced in $CST^{-/-}$ mice (Figs. 4 and S6). Previously, we proposed that MAG and NF155 do not anchor in/associate with the membrane appropriately, which resulted in easier detergent extraction (Pomicter *et al.* 2013). Our new data are consistent with such a notion. We further proposed that the impaired association between MAG/NF155 and the myelin membrane in the absence of ST leads to faster turnover/degradation of these proteins.

Given that MAG is exclusively localized in the innermost periaxonal membrane of myelin internodes in the CNS (Trapp *et al.* 1989) and that the paranodal protein NF155 mediates the myelin-axon junction by directly interacting with the axonal heterocomplex of contactin-associated protein (Caspr) and contactin (Charles *et al.* 2002; Bonnon *et al.* 2007), our findings provide a molecular basis for the described effects of ST on glial-axon signaling, including nodal and paranodal deterioration, uncompacted myelin, vacuolar degeneration (Marcus *et al.* 2006), as well as the abnormal localization and maintenance of sodium and

potassium ion channel clusters in adult CST-depleted mice (Ishibashi *et al.* 2002). Consistent with the temporal effect of ST deficiency on MAG content (Fig. S6c), vacuolar degeneration was rare in 1-month-old $CST^{-/-}$ mice, which also displayed normal node lengths and proper ion channel clusters. On the other hand, aged knockout mice displayed frequent vacuolar degeneration and abnormal paranodes, as well as longer nodes and abnormal channel clusters (Ishibashi et al. 2002; Marcus et al. 2006).

Proposed molecular mechanisms underlying the effects of ST depletion on myelin structure/function

Sulfatides are the only major negatively-charged lipids present in the outer leaflet of myelin membrane (Fig. 7a). Moreover, it is well established that the positively charged compact myelin proteins interact with the negatively charged membrane lipids to stabilize the major dense line of CNS myelin (Siegel *et al.* 1999) (Fig. 7a). Therefore, the loss of ST species will certainly result in major charge alterations between outer and inner membrane leaflets and will alter the balance between positively charged compact-myelin proteins and negatively charged myelin membrane lipids. We proposed a model in which under ST-depleted conditions the loss of negative membrane lipid charges is compensated by an early and significant decrease in the positively charged compact myelin proteins. In other words, we proposed that OLs compensate the reduction of negative charges in the myelin membrane by reducing the levels of the positively charged compact myelin proteins in order to maintain the proper charge balance required for myelin stability. Furthermore, our data strongly support a mechanism in which the reduction of ST has an effect of global lipid synthesis in OLs. The loss of both myelin lipids and compact-myelin proteins provide a molecular foundation for the thinner myelin sheaths reported in our ultrastructural studies on ST-depleted mice which were ~30% thinner than those of wildtype mice (Fig. 7b, green). Importantly, $CGT^{-/-}$, also showed myelin sheaths that are about 70% as thick as the controls (Coetzee *et al.* 1996). Given that a similar effect was seen in $CST^{-/-}$ mice (Marcus *et al.* 2006), the lack of ST (not of GalCer) seems to be the major driver of this myelin loss. In addition, given that GalCer is neutral, the charge effects proposed above would be specific to the loss of ST.

ST depletion led to dramatic inner myelin tongue and paranodal alterations (evidenced by the dramatic decrease in MAG and NF155, respectively), but had no consequences on the outer myelin tongue (evidenced by physiological levels of MOG). We proposed that the basis of this selectivity relies on the association between specific proteins and the membrane in the presence or absence of ST. Our model states that in the absence of ST, MAG and NF155 are loosely bound to the myelin membrane; while in the presence of ST, MAG and NF155 are strongly anchored/associated within the myelin membrane. The sulfate group of ST presumably stabilizes such interactions either through its negative charge or its polarity. Thus, in the absence of ST, the loosely membrane-bound MAG and NF155 are more susceptible to degradation, and are consequently prone to degradation following myelin development (Fig. 7b, gray).

Careful examination revealed that the HMW PLP dimer/oligomers bands decreased in a progressive and age-dependent manner (Fig. S6e–f). Importantly, the lipophilic amino acid

tryptophan, present on the outer surface edge of PLP has been predicted to interact with galactosphingolipids of the outer lipid membrane of the adjacent myelin spiral (Coetzee *et al.* 1998). This study strongly supports such a prediction, and proposes that the galactosphingolipid responsible for mediating and/or stabilizing PLP interactions is ST. We proposed that the progressive loss of intermolecular PLP interactions represents the molecular basis behind the increased uncompacted myelin and cytoplasmic islands within regions of otherwise compact myelin in aged $CST^{-/-}$ mice (Fig. 7b, purple).

As previously described, $CST^{-/-}$ mice develop a tremor phenotype that becomes evident by 4–6 weeks of age and further aggravates with age. Despite the fact that ST depletion led to significant reductions of myelin lipids (Figs. 1–3), major compact and non-compact myelin proteins (Figs. 4–5 and S6), and myelin thickness (Marcus *et al.* 2006) (Fig. 6), such effects were not progressive and therefore do not seem to be capable of explaining the tremor/ataxic phenotype that exacerbates with age in $CST^{-/-}$ mice. Supporting this notion is the fact that multiple mouse models have been reported to display a significant reduction in myelin thickness but do not develop tremors (Ishii *et al.* 2014; Hu *et al.* 2006). In addition, transient expression of MBP content in $MBP^{-/-}$ mice demonstrated that restoring ~50% of myelin thickness was sufficient to rescue their tremor phenotype (Popko *et al.* 1987; Readhead *et al.* 1987; Shine *et al.* 1992). Similarly, the effect of ST depletion on MAG levels do not seem to be responsible for the tremor phenotype since MAG downregulation did not progress as adult mice aged, and more convincingly, $MAG^{-/-}$ mice do not tremor (Bartsch *et al.* 1997).

We proposed that the dramatic and progressive loss of NF155 and PLP interactions are the molecular basis underlying the progressive tremor/ataxic phenotype characteristic of $CST^{-/-}$ mice. This idea is strongly supported by the fact that paranodal deterioration and the extent of uncompacted myelin in $CST^{-/-}$ mice also aggravate with age (Marcus *et al.* 2006). More importantly, a recently developed strain of $NF155^{-/-}$ mice displayed notable postnatal tremors (Roche *et al.* 2014), showing that the loss of NF155 by itself can lead to a tremor phenotype. In addition, research related to Pelizaeus-Merzbacher disease (PMD), a dysmyelinating disease caused by mutations in the PLP gene, has shown that PMD patients typically develop tremors due to the mislocalization of PLP (Dhaunchak & Nave 2007). PLP mutant forms rapidly assemble dimers/oligomers at the ER and not in the myelin membrane (Dhaunchak & Nave 2007). Thus, the lack of intermolecular PLP interactions at the myelin membrane by itself also seems to lead to the tremor phenotype. In summary, we proposed that the aggravating tremor and ataxic phenotypes under ST depleted conditions occur as a consequence of the loss of NF155 and PLP intermolecular interactions, resulting in the disruption of the myelin-axon junction and the myelin intraperiod line. Our model is consistent with the onset of the tremor phenotype, which as previously stated becomes evident by 6 weeks of age, and progressively aggravates reaching partial hindlimb ataxia at ≥10 months.

Supplementary Material

Refer to Web version on PubMed Central for supplementary material.

Acknowledgments

This work was partly supported by the National Institute of General Medical Sciences Grant R01 GM105724, American Diabetes Association Grant #7-15-MI-07, and intramural institutional research funds. Histological and confocal microscopy analysis was performed at the Histology and Cell Imaging Core at SBP Medical Discovery Institute.

List of abbreviations

CST	Cerebroside sulfotransferase
CNP	cyclic nucleotide phosphodiesterase
FA	fatty acid
GalCer	galactosylceramide
LPLs	lysophospholipids
MLD	metachromatic leukodystrophy
MDMS-SL	multi-dimensional mass spectrometry-based shotgun lipidomics
MAG	myelin-associated glycoprotein
MBP	myelin basic protein
MOG	myelin-oligodendrocyte glycoprotein
SirT2	NAD-dependent deacetylase sirtuin-2
NF	neurofascin
OL	oligodendrocyte
PLS-DA	partial least square-discriminate analysis
PMD	Pelizaeus-Merzbacher disease
PC	phosphatidylcholine
PE	phosphatidylethanolamine
PS	phosphatidylserine
PLP	proteolipid protein
SM	sphingomyelin
ST	sulfatide

REFERENCES

Bansal R, Gard AL, Pfeiffer SE. Stimulation of oligodendrocyte differentiation in culture by growth in the presence of a monoclonal antibody to sulfated glycolipid. J Neurosci Res. 1988; 21:260–267. [PubMed: 2464078]

Bansal R, Pfeiffer SE. Reversible inhibition of oligodendrocyte progenitor differentiation by a monoclonal antibody against surface galactolipids. Proc Natl Acad Sci U S A. 1989; 86:6181–6185. [PubMed: 2668957]

Bansal R, Winkler S, Bheddah S. Negative regulation of oligodendrocyte differentiation by galactosphingolipids. J Neurosci. 1999; 19:7913–7924. [PubMed: 10479693]

Bartsch S, Montag D, Schachner M, Bartsch U. Increased number of unmyelinated axons in optic nerves of adult mice deficient in the myelin-associated glycoprotein (MAG). Brain Res. 1997; 762:231–234. [PubMed: 9262180]

Benjamins JA, Morell P. Proteins of myelin and their metabolism. Neurochem Res. 1978; 3:137–174. [PubMed: 353578]

Boggs JM, Wang H. Effect of liposomes containing cerebroside and cerebroside sulfate on cytoskeleton of cultured oligodendrocytes. J Neurosci Res. 2001; 66:242–253. [PubMed: 11592120]

Bonnon C, Bel C, Goutebroze L, Maigret B, Girault JA, Faivre-Sarrailh C. PGY repeats and N-glycans govern the trafficking of paranodin and its selective association with contactin and neurofascin-155. Mol Biol Cell. 2007; 18:229–241. [PubMed: 17093057]

Campagnoni AT, Skoff RP. The pathobiology of myelin mutants reveal novel biological functions of the MBP and PLP genes. Brain Pathol. 2001; 11:74–91. [PubMed: 11145205]

Charles P, Tait S, Faivre-Sarrailh C, et al. Neurofascin is a glial receptor for the paranodin/Caspr-contactin axonal complex at the axoglial junction. Curr Biol. 2002; 12:217–220. [PubMed: 11839274]

Cheng H, Guan S, Han X. Abundance of triacylglycerols in ganglia and their depletion in diabetic mice: implications for the role of altered triacylglycerols in diabetic neuropathy. J Neurochem. 2006; 97:1288–1300. [PubMed: 16539649]

Cheng H, Jiang X, Han X. Alterations in lipid homeostasis of mouse dorsal root ganglia induced by apolipoprotein E deficiency: a shotgun lipidomics study. J Neurochem. 2007; 101:57–76. [PubMed: 17241120]

Cheng H, Zhou Y, Holtzman DM, Han X. Apolipoprotein E mediates sulfatide depletion in animal models of Alzheimer's disease. Neurobiol Aging. 2010; 31:1188–1196. [PubMed: 18762354]

Chrast R, Saher G, Nave KA, Verheijen MH. Lipid metabolism in myelinating glial cells: lessons from human inherited disorders and mouse models. J Lipid Res. 2011; 52:419–434. [PubMed: 21062955]

Coetzee T, Fujita N, Dupree J, Shi R, Blight A, Suzuki K, Suzuki K, Popko B. Myelination in the absence of galactocerebroside and sulfatide: normal structure with abnormal function and regional instability. Cell. 1996; 86:209–219. [PubMed: 8706126]

Coetzee T, Suzuki K, Popko B. New perspectives on the function of myelin galactolipids. Trends Neurosci. 1998; 21:126–130. [PubMed: 9530920]

Daffu G, Sohi J, Kamholz J. Proteolipid protein dimerization at cysteine 108: Implications for protein structure. Neurosci Res. 2012; 74:144–155. [PubMed: 22902553]

Dhaunchak AS, Nave KA. A common mechanism of PLP/DM20 misfolding causes cysteine-mediated endoplasmic reticulum retention in oligodendrocytes and Pelizaeus-Merzbacher disease. Proc Natl Acad Sci U S A. 2007; 104:17813–17818. [PubMed: 17962415]

Dyer CA, Benjamins JA. Antibody to galactocerebroside alters organization of oligodendroglial membrane sheets in culture. J Neurosci. 1988; 8:4307–4318. [PubMed: 2460596]

Eckhardt M, Hedayati KK, Pitsch J, Lullmann-Rauch R, Beck H, Fewou SN, Gieselmann V. Sulfatide storage in neurons causes hyperexcitability and axonal degeneration in a mouse model of metachromatic leukodystrophy. J Neurosci. 2007; 27:9009–9021. [PubMed: 17715338]

Fewou SN, Fernandes A, Stockdale K, Francone VP, Dupree JL, Rosenbluth J, Pfeiffer SE, Bansal R. Myelin protein composition is altered in mice lacking either sulfated or both sulfated and non-sulfated galactolipids. J Neurochem. 2010; 112:599–610. [PubMed: 19878436]

Foran DR, Peterson AC. Myelin acquisition in the central nervous system of the mouse revealed by an MBP-Lac Z transgene. J Neurosci. 1992; 12:4890–4897. [PubMed: 1281497]

Greer JM, Lees MB. Myelin proteolipid protein--the first 50 years. Int J Biochem Cell Biol. 2002; 34:211–215. [PubMed: 11849988]

Han X. Potential mechanisms contributing to sulfatide depletion at the earliest clinically recognizable stage of Alzheimer's disease: a tale of shotgun lipidomics. J Neurochem. 2007; 103(Suppl 1):171–179. [PubMed: 17986152]

Han, X. Lipidomics: Comprehensive mass spectrometry of lipids. Hoboken, New Jersey: John Wiley & Sons, Inc.; 2016.

Han X, Cheng H, Fryer JD, Fagan AM, Holtzman DM. Novel role for apolipoprotein E in the central nervous system. Modulation of sulfatide content. J Biol Chem. 2003; 278:8043–8051. [PubMed: 12501252]

Han X, Gross RW. Shotgun lipidomics: multidimensional MS analysis of cellular lipidomes. Expert Rev Proteomics. 2005; 2:253–264. [PubMed: 15892569]

Han X, Holtzman DM, McKeel DW Jr. Plasmalogen deficiency in early Alzheimer's disease subjects and in animal models: molecular characterization using electrospray ionization mass spectrometry. J Neurochem. 2001; 77:1168–1180. [PubMed: 11359882]

Han X, Holtzman DM, McKeel DW Jr, Kelley J, Morris JC. Substantial sulfatide deficiency and ceramide elevation in very early Alzheimer's disease: potential role in disease pathogenesis. J Neurochem. 2002; 82:809–818. [PubMed: 12358786]

Han X, Yang K, Gross RW. Microfluidics-based electrospray ionization enhances the intrasource separation of lipid classes and extends identification of individual molecular species through multi-dimensional mass spectrometry: development of an automated high-throughput platform for shotgun lipidomics. Rapid Commun Mass Spectrom. 2008; 22:2115–2124. [PubMed: 18523984]

Han X, Yang K, Gross RW. Multi-dimensional mass spectrometry-based shotgun lipidomics and novel strategies for lipidomic analyses. Mass Spectrom Rev. 2012; 31:134–178. [PubMed: 21755525]

Hayashi A, Kaneko N, Tomihira C, Baba H. Sulfatide decrease in myelin influences formation of the paranodal axo-glial junction and conduction velocity in the sciatic nerve. Glia. 2013; 61:466–474. [PubMed: 23322453]

Hirahara Y, Bansal R, Honke K, Ikenaka K, Wada Y. Sulfatide is a negative regulator of oligodendrocyte differentiation: development in sulfatide-null mice. Glia. 2004; 45:269–277. [PubMed: 14730700]

Honke K, Hirahara Y, Dupree J, et al. Paranodal junction formation and spermatogenesis require sulfoglycolipids. Proc Natl Acad Sci U S A. 2002; 99:4227–4232. [PubMed: 11917099]

Hu X, Hicks CW, He W, Wong P, Macklin WB, Trapp BD, Yan R. Bace1 modulates myelination in the central and peripheral nervous system. Nat Neurosci. 2006; 9:1520–1525. [PubMed: 17099708]

Ishibashi T, Dupree JL, Ikenaka K, et al. A myelin galactolipid, sulfatide, is essential for maintenance of ion channels on myelinated axon but not essential for initial cluster formation. J Neurosci. 2002; 22:6507–6514. [PubMed: 12151530]

Ishii A, Furusho M, Dupree JL, Bansal R. Role of ERK1/2 MAPK signaling in the maintenance of myelin and axonal integrity in the adult CNS. J Neurosci. 2014; 34:16031–16045. [PubMed: 25429144]

Kriebel M, Wuchter J, Trinks S, Volkmer H. Neurofascin: a switch between neuronal plasticity and stability. Int J Biochem Cell Biol. 2012; 44:694–697. [PubMed: 22306302]

Marcus J, Dupree JL, Popko B. Effects of galactolipid elimination on oligodendrocyte development and myelination. Glia. 2000; 30:319–328. [PubMed: 10797612]

Marcus J, Honigbaum S, Shroff S, Honke K, Rosenbluth J, Dupree JL. Sulfatide is essential for the maintenance of CNS myelin and axon structure. Glia. 2006; 53:372–381. [PubMed: 16288467]

Norton WT, Poduslo SE. Myelination in rat brain: changes in myelin composition during brain maturation. J Neurochem. 1973; 21:759–773. [PubMed: 4754856]

Pomicter AD, Deloyht JM, Hackett AR, Purdie N, Sato-Bigbee C, Henderson SC, Dupree JL. Nfasc155H and MAG are specifically susceptible to detergent extraction in the absence of the myelin sphingolipid sulfatide. Neurochem Res. 2013; 38:2490–2502. [PubMed: 24081651]

Pomicter AD, Shroff SM, Fuss B, Sato-Bigbee C, Brophy PJ, Rasband MN, Bhat MA, Dupree JL. Novel forms of neurofascin 155 in the central nervous system: alterations in paranodal disruption models and multiple sclerosis. Brain. 2010; 133:389–405. [PubMed: 20129933]

Popko B, Puckett C, Lai E, Shine HD, Readhead C, Takahashi N, Hunt SW 3rd, Sidman RL, Hood L. Myelin deficient mice: expression of myelin basic protein and generation of mice with varying levels of myelin. Cell. 1987; 48:713–721. [PubMed: 2434243]

Quarles RH. Myelin-associated glycoprotein (MAG): past, present and beyond. J Neurochem. 2007; 100:1431–1448. [PubMed: 17241126]

Rasband MN, Tayler J, Kaga Y, Yang Y, Lappe-Siefke C, Nave KA, Bansal R. CNP is required for maintenance of axon-glia interactions at nodes of Ranvier in the CNS. Glia. 2005; 50:86–90. [PubMed: 15657937]

Readhead C, Popko B, Takahashi N, Shine HD, Saavedra RA, Sidman RL, Hood L. Expression of a myelin basic protein gene in transgenic shiverer mice: correction of the dysmyelinating phenotype. Cell. 1987; 48:703–712. [PubMed: 2434242]

Roche SL, Sherman DL, Dissanayake K, et al. Loss of glial neurofascin155 delays developmental synapse elimination at the neuromuscular junction. J Neurosci. 2014; 34:12904–12918. [PubMed: 25232125]

Roth MP, Malfroy L, Offer C, Sevin J, Enault G, Borot N, Pontarotti P, Coppin H. The human myelin oligodendrocyte glycoprotein (MOG) gene: complete nucleotide sequence and structural characterization. Genomics. 1995; 28:241–250. [PubMed: 8530032]

Shine HD, Readhead C, Popko B, Hood L, Sidman RL. Morphometric analysis of normal, mutant, and transgenic CNS: correlation of myelin basic protein expression to myelinogenesis. J Neurochem. 1992; 58:342–349. [PubMed: 1370079]

Shroff SM, Pomicter AD, Chow WN, Fox MA, Colello RJ, Henderson SC, Dupree JL. Adult CST-null mice maintain an increased number of oligodendrocytes. J Neurosci Res. 2009; 87:3403–3414. [PubMed: 19224580]

Siegel GJ, Agranoff BW, Albers RW, et al. Basic Neurochemistry: Moelcular, Cellular and Medical Aspects (6th). 1999; Chapter 4 Vol.

Southwood CM, Peppi M, Dryden S, Tainsky MA, Gow A. Microtubule deacetylases, SirT2 and HDAC6, in the nervous system. Neurochem Res. 2007; 32:187–195. [PubMed: 16933150]

Svennerholm L, Gottfries CG. Membrane lipids, selectively diminished in Alzheimer brains, suggest synapse loss as a primary event in early-onset form (type I) and demyelination in late-onset form (type II). J Neurochem. 1994; 62:1039–1047. [PubMed: 8113790]

Swanton E, Holland A, High S, Woodman P. Disease-associated mutations cause premature oligomerization of myelin proteolipid protein in the endoplasmic reticulum. Proc Natl Acad Sci U S A. 2005; 102:4342–4347. [PubMed: 15753308]

Takahashi T, Suzuki T. Role of sulfatide in normal and pathological cells and tissues. J Lipid Res. 2012; 53:1437–1450. [PubMed: 22619219]

Trapp BD, Andrews SB, Cootauco C, Quarles R. The myelin-associated glycoprotein is enriched in multivesicular bodies and periaxonal membranes of actively myelinating oligodendrocytes. J Cell Biol. 1989; 109:2417–2426. [PubMed: 2478568]

Wang C, Wang M, Zhou Y, Dupree JL, Han X. Alterations in mouse brain lipidome after disruption of CST gene: a lipidomics study. Mol Neurobiol. 2014; 50:88–96. [PubMed: 24395133]

Wang M, Wang C, Han RH, Han X. Novel advances in shotgun lipidomics for biology and medicine. Prog Lipid Res. 2016a; 61:83–108. [PubMed: 26703190]

Wang M, Wang C, Han X. Selection of internal standards for accurate quantification of complex lipid species in biological extracts by electrospray ionization mass spectrometry-What, how and why? Mass Spectrom Rev. 2016b

Yang K, Cheng H, Gross RW, Han X. Automated lipid identification and quantification by multidimensional mass spectrometry-based shotgun lipidomics. Anal Chem. 2009; 81:4356–4368. [PubMed: 19408941]

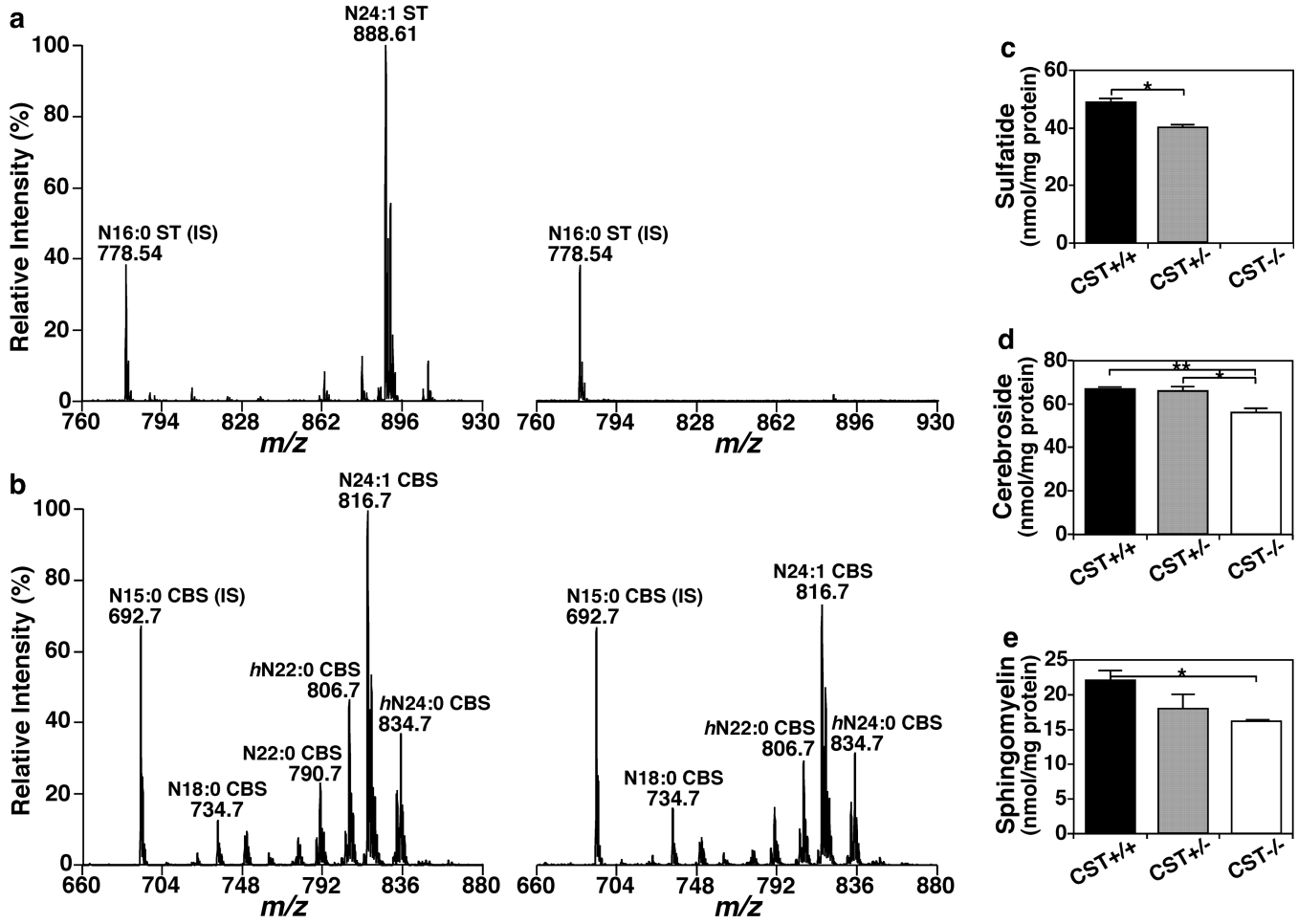

Fig. 1.

The effect of CST disruption on sphingolipid homeostasis in the spinal cord of adult mice. Mouse spinal cords from 3-months old CST male mice were homogenized followed by modified Bligh and Dyer lipid extraction. Representative mass spectra from $CST^{+/+}$ (left) and $CST^{-/-}$ (right) mice were shown for sulfatides (a) and sphingomyelins (b). Total masses of the major sphingolipid classes present in myelin were quantified by MDMS-SL as described in the section of “Materials and Methods” and plotted. Total sulfatide (c), cerebroside (d), and sphingomyelin (e) contents of CST+/+ (black bars), +/− (gray bars) and −/− (white bars) spinal cords represent the sum of all the individual lipid species detected within each genotype. The data represent means ± SE from at least 4 separate animals. *$p <$ 0.05 and **$p < 0.01$ as indicated.

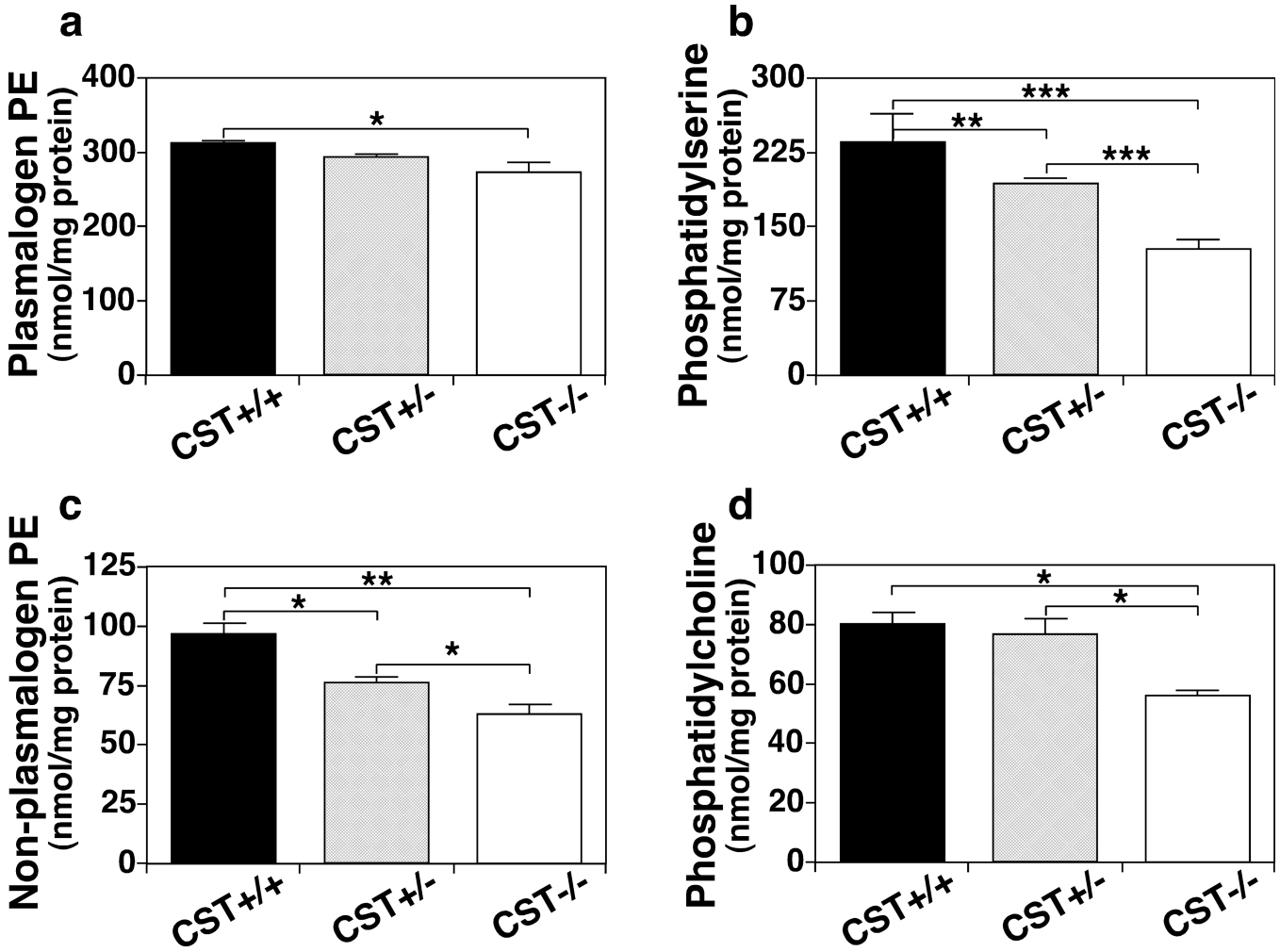

Fig. 2.

The effect of CST disruption on phospholipid homeostasis in the spinal cord of adult mice. Mouse spinal cords from 3-month old CST male mice were homogenized followed by modified Bligh and Dyer lipid extraction. Total masses for the major phospholipid classes present in myelin were quantified by MDMS-SL as described in the section of “Materials and Methods” and plotted. Total plasmalogen PE (a), phosphatidylserine (b), non-plasmalogen PE (c), and phosphatidylcholine (d) contents of CST+/+ (black bars), +/− (gray bars) and −/− (white bars) spinal cords represent the sum of all the individual lipid species detected within each genotype. The data represent means ± SE from at least 4 separate animals. *$p < 0.05$, **$p < 0.01$, and ***$p < 0.001$ as indicated.

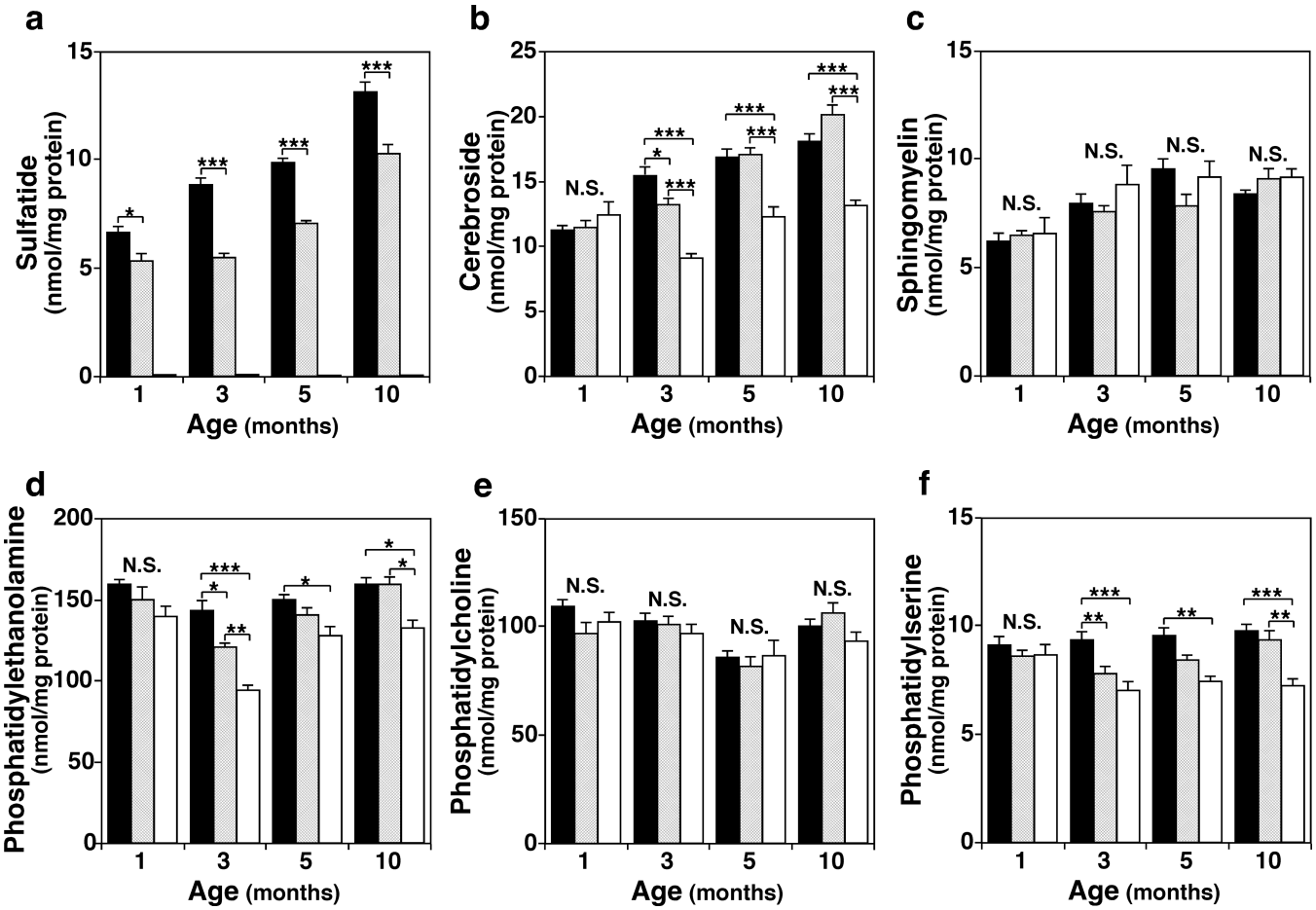

Fig. 3.

Longitudinal effects of CST disruption on sphingolipid and phospholipid homeostasis in adult mouse brains. Cerebella from 1-, 3-, 5-, and 10-months old CST male mice were homogenized followed by modified Bligh and Dyer lipid extraction. Total masses for the major sphingolipid (a–c) and phospholipid (e–f) classes present in CST+/+ (black bars), +/− (gray bars), and −/− (white bars) cerebella were quantified by MDMS-SL as described in the section of "Materials and Methods" and plotted. The data represent means ± SE from at least 4 separate animals. N.S. no significant difference, *$p < 0.05$, **$p < 0.01$, and ***$p < 0.001$ as indicated.

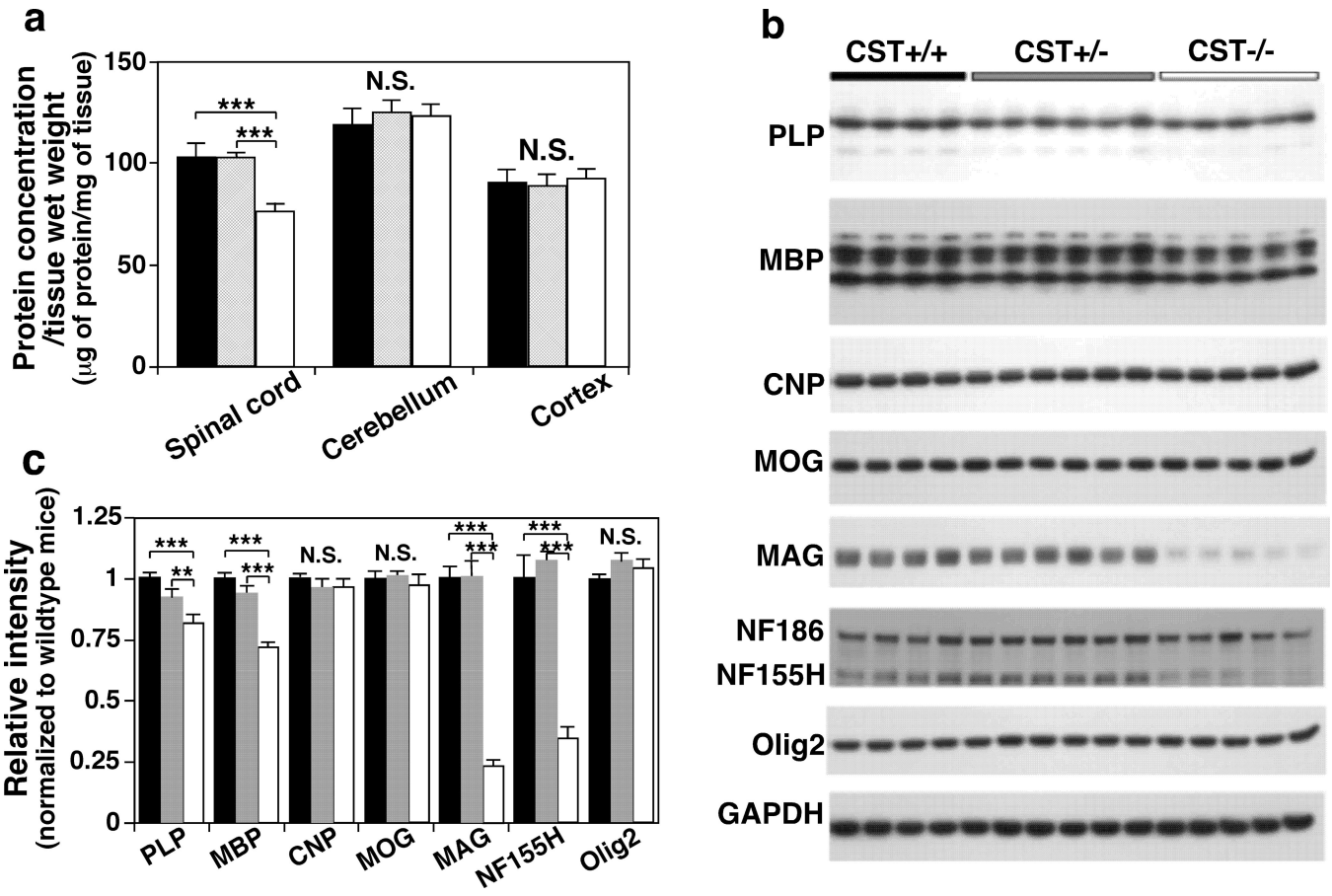

Fig. 4.

The effect of CST disruption on the levels of major CNS myelin proteins. Mouse spinal cord, cerebellum, and cortical tissue from 3-month old CST+/+ (black bars), +/− (gray bars), and −/− (white bars) male mice were homogenized and its total protein concentration was estimated by BCA protein assay (a). Representative Western blots from cerebellar NP40 supernatants using antibodies against PLP, MBP, CNP, MOG, MAG, NF, GAPDH, and Olig2 (b). Relative intensities were quantified using *ImageJ* software and normalized to a loading control (GAPDH) (c). The data represent means ± SE from at least 4 separate animals. N.S. denotes no significant difference, $*p < 0.05$ and $***p < 0.001$ as indicated.

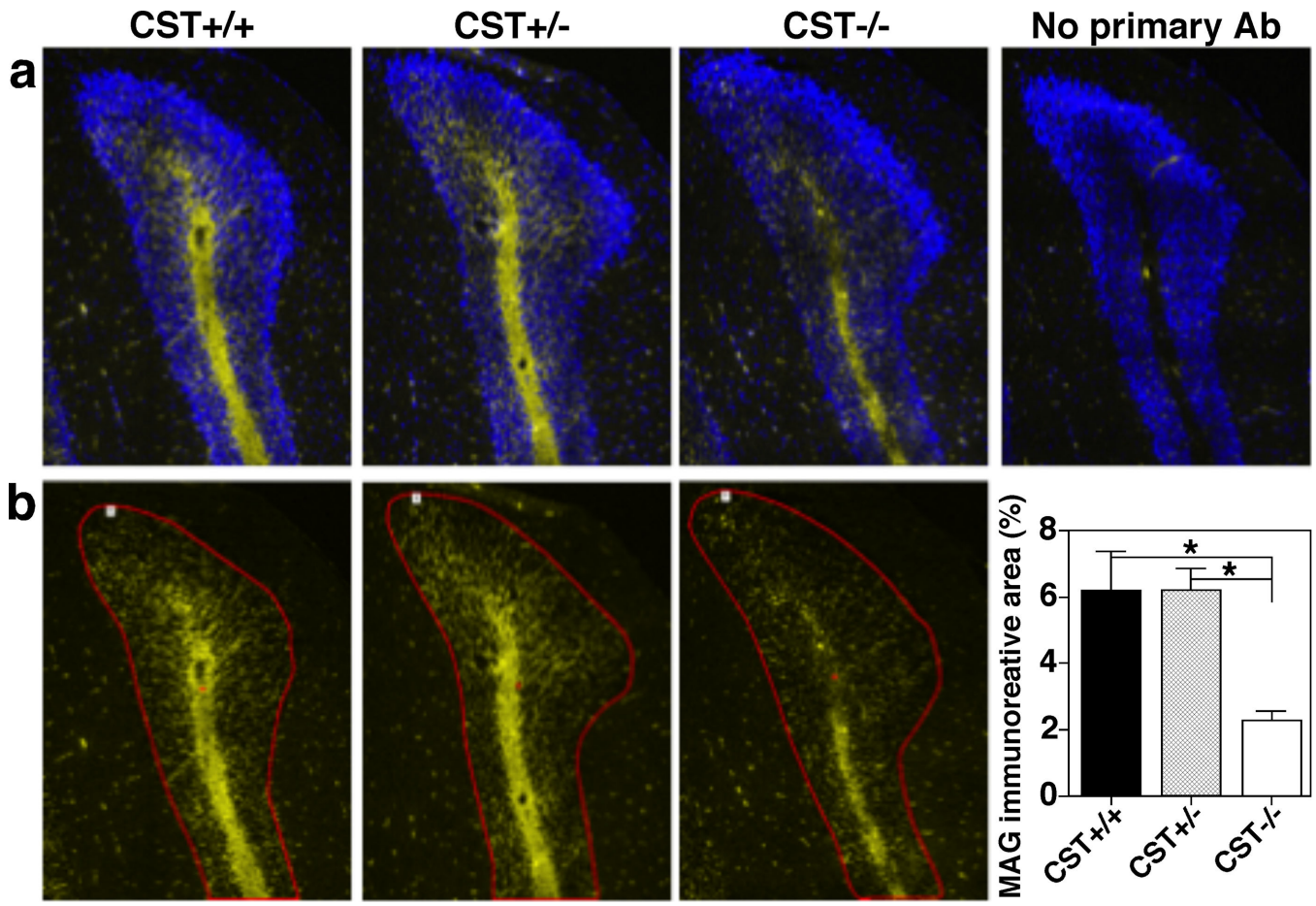

Fig. 5.

Sulfatide deficiency leads to a dramatic decrease of MAG. CST+/+ (left), +/− (middle), and −/− (right) mouse brains were dissected, fixed in 4% PFA, cryoprotected, frozen, and sectioned coronally (8 μm sections). Representative immunofluorescence images from cerebellar coronal sections (posterior lobe) using anti-MAG antibody (rabbit mAb, Cell Signaling) were shown merged with DAPI (a) and individually (b). Yellow and blue signals represent positive MAG and DAPI staining, respectively. Regions of interest (ROI) were defined within single cerebellar folium using the cerebellar Purkinje layer as its border (ROI 1, red) and the area of immunoreactivity above a threshold was quantified (such threshold was defined based on the control conducted without any primary antibody, shown in the top right). Three equally spaced cerebellar sections were quantified for each individual. The data represent means ± SE from 4 separate animals. *$p < 0.05$, as indicated.

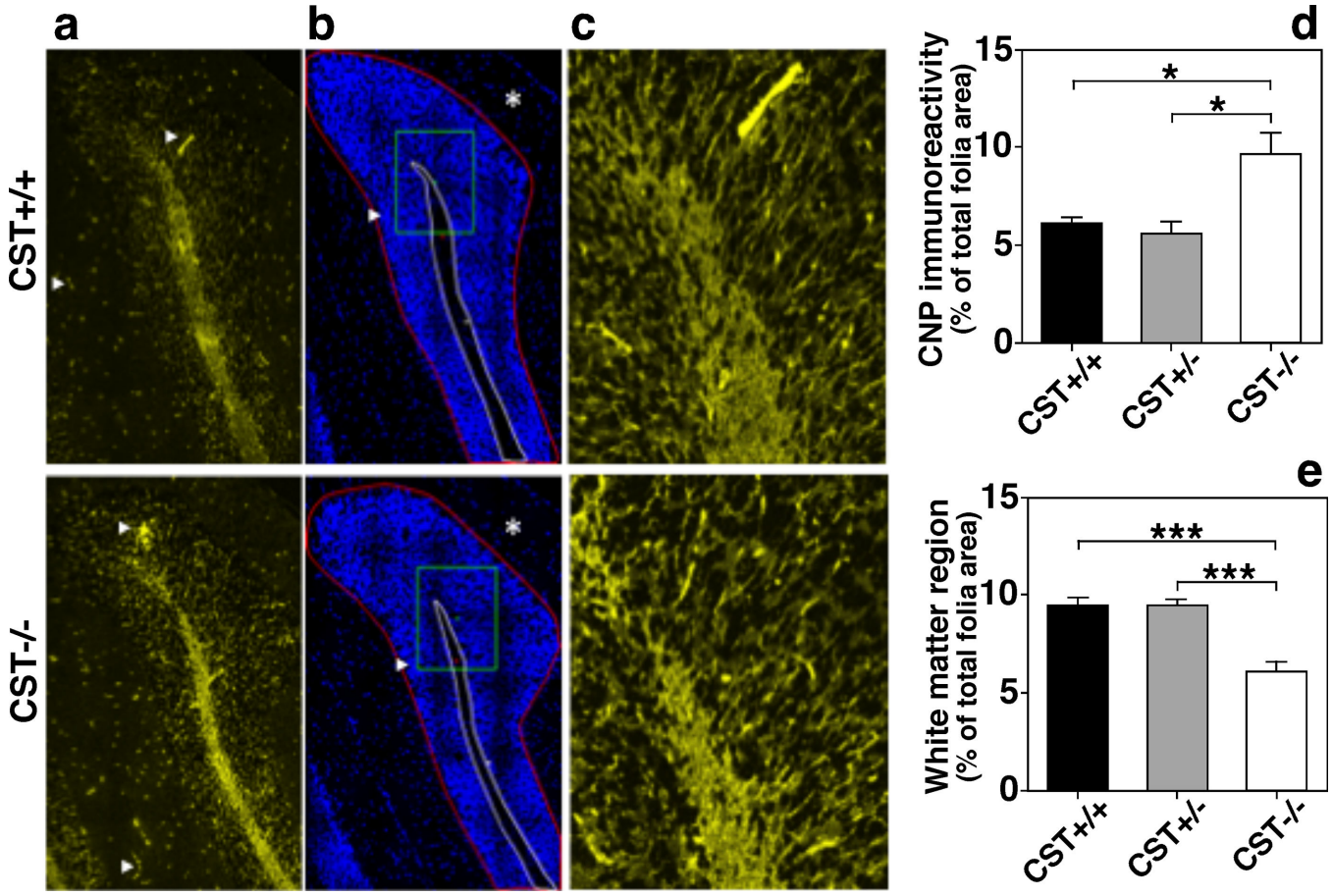

Fig. 6.

Sulfatide deficiency leads to thinner white matter tracks with a dense population of oligodendrocytes. CST+/+ (top color panels) and −/− (bottom color panels) mouse brains were dissected, fixed in 4% PFA, cryoprotected, frozen, and sectioned coronally (8 μm sections). Representative immunofluorescence images were taken from equivalent cerebellar coronal sections (posterior cerebellar lobe) using anti-CNP (rabbit mAb, Cell Signaling; a and c). DAPI staining (b) is also shown. The images were taken using 40× (a–b) and 60× (c) objectives on a Nikon A1R VAAS inverted confocal. Yellow and blue signals represent positive CNP and DAPI staining, respectively. A non-specific autofluorescence signal was observed in the yellow channel within blood vessels (presumably due to the fact that the animals were not perfused given that their brain tissue was used for multiple purposes) Two regions of interest (ROI) were defined: 1. the area delimited by the Purkinje layer including the granular layer and white matter (ROI1, area defined by red border in b), 2. white matter (ROI2, area defined by white border in b). The area of immunoreactivity above a defined threshold was quantified for CNP (d) using ROI2. White matter area (ROI2) was quantified as a percent of the total folia area (ROI1) (e). Three equally spaced cerebellar sections were quantified for each individual. The data represent means ± SE from 4 separate animals. *$p < 0.05$, ***$p < 0.001$ as indicated.

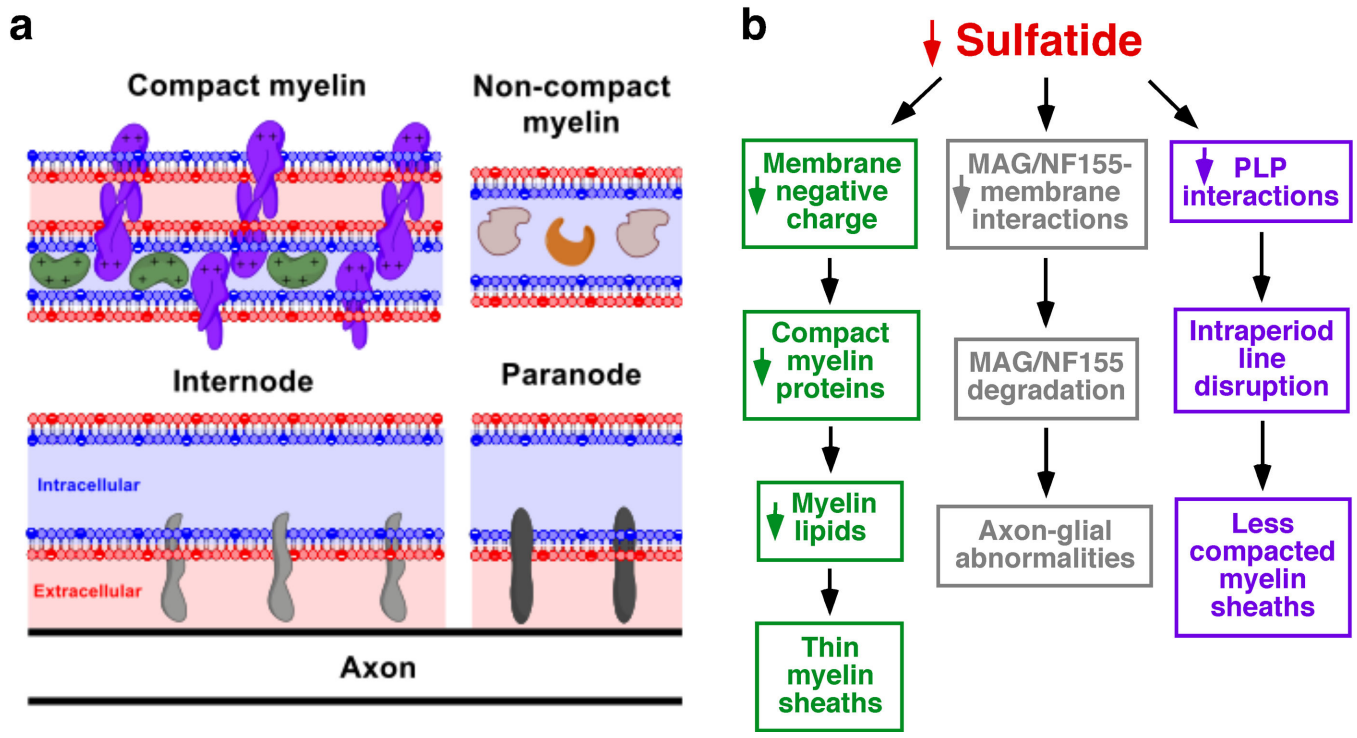

Fig. 7.

Molecular mechanisms by which sulfatide regulates myelin maintenance and function. (a) Schematic representation of compact and inner tongue myelin membranes. Sulfatide is depicted as filled, negatively charged red circles within the outer membrane leaflet. Negatively charged inner membrane leaflet lipids (e.g., PS) are depicted as filled blue circles within the inner membrane leaflet. Major myelin proteins such as MBP (green), PLP (purple), MAG (light gray), NF155 (dark gray), CNP (brown), and SirT2 (orange) were schematically illustrated. (b) Three major molecular mechanisms by which sulfatide depletion leads to thinner myelin sheaths, axon-glial abnormalities, and less compacted myelin sheaths were summarized.